\(A\beta\) alters the connectivity of olfactory neurons in the absence of amyloid plaques in vivo

Published in final edited form as:
Nat Commun. 2012 ; 3: 1009. doi:10.1038/ncomms2013.

Aβ alters the connectivity of olfactory neurons in the absence of amyloid plaques *in vivo*

Luxiang Cao[1], **Benjamin R. Schrank**[1], **Steve Rodriguez**[1], **Eric G. Benz**[1], **Thomas W. Moulia**[1], **Gregory T. Rickenbacher**[1], **Alexis C. Gomez**[1], **Yona Levites**[2], **Sarah R. Edwards**[1], **Todd E. Golde**[2], **Bradley T. Hyman**[1], **Gilad Barnea**[3], and **Mark W. Albers**[1,*]

[1]MassGeneral Institute of Neurodegenerative Disease, Dept. of Neurology, Harvard Medical School, Boston, MA 02129

[2]Dept. of Neuroscience, University of Florida, Gainesville, FL 32610

[3]Dept. of Neuroscience, Brown University, Providence, RI 02912

Abstract

The Aβ peptide aggregates into amyloid plaques at presymptomatic stages of Alzheimer's disease, but the temporal relationship between plaque formation and neuronal dysfunction is poorly understood. Here, we demonstrate that the connectivity of the peripheral olfactory neural circuit is perturbed in mice overexpressing human APPsw (Swedish mutation) prior to the onset of plaques. Expression of hAPPsw exclusively in olfactory sensory neurons (OSNs) also perturbs connectivity with associated reductions in odor-evoked gene expression and olfactory acuity. By contrast, OSN axons project correctly in mice overexpressing wild type human APP throughout the brain and in mice overexpressing human APPmv, a missense mutation that reduces Aβ production, exclusively in OSNs. Furthermore, expression of Aβ40 or Aβ42 solely in the olfactory epithelium disrupts OSN axon targeting. Our data indicate that altering the structural connectivity and function of highly plastic neural circuits is one of the pleiotropic actions of soluble human Aβ.

The pathobiology of Alzheimer's disease (AD) erodes neural networks and their underlying neural circuits, resulting in cognitive deficits and, ultimately, dementia[1]. Accumulations of Aβ peptide assemblies in the cortex, especially amyloid plaques, are present years prior to the onset of clinical symptoms of AD[2]. In fact, approximately thirty percent of cognitively intact septuagenarians harbor cerebral amyloid plaques[3, 4]. Defining the temporal relationship between neural network dysfunction and amyloid deposition is crucial to developing effective therapies for the preclinical stage of AD[5].

Transgenic mice overexpressing pathogenic mutated alleles of the human amyloid precursor protein (APP) model the cerebral amyloidosis of preclinical AD[6]. In these models, neurons surrounding amyloid plaques exhibit reduced dendritic spine density and elevated resting

*Correspondence should be addressed to: Mark W. Albers, MassGeneral Institute of Neurodegenerative Disease, 114 16th St. #2003, Boston, MA 02129 T: 617-724-7401 F: 617-724-1480 albers.mark@mgh.harvard.edu.

Author Contributions

L.C., S.R., and M.W.A. designed the research, L.C., B.R.S., S.R., E.G.B., T.W.M., G.T.R., A.C.G., Y.L., S.R.E., and M.W.A. performed experiments, T.E.G., B.T.H., and G.B. contributed new reagents and analytic tools, L.C., B.R.S., S.R., E.G.B., T.W.M., G.T.R., and M.W.A. analyzed data, M.W.A. wrote the initial draft, all authors reviewed and revised the paper.

Competing Financial Interests

T.E.G. has received support from Myriad Genetics and Lunkbeck, Inc. T.E.G. has consulted for Elan, Lundbeck Inc., Sonexa Therapeutics, and Kareus Therapeutics. B.T.H. has consulted for EMD Serrano, Janssen, Takeda, BMS, Neurophage, Pfizer, Quanterix, foldrx, Elan, and Link.

intracellular calcium concentrations[7, 8]. However, loss of synaptic proteins precede amyloid deposition in these models[9], and soluble Aβ species disrupt neural network function, e.g, inhibiting long-term potentiation, inducing long-term depression (LTD), and diminishing the density of dendritic spines[10, 11]. Lentiviral expression of hAPP, but not hAPPmv (M671V, a synthetic missense mutation of hAPP which impairs Aβ generation[12]), in hippocampal slice preparations evoked a LTD-like phenotype and reduced spine density in adjacent neurons not expressing hAPP[13-15]. Together, these data indicate that soluble Aβ species, either released from cells or diffusing from the periphery of amyloid deposits, mediate neural circuit dysfunction.

In this study we probe the actions of human Aβ in the mouse peripheral olfactory neural circuit *in vivo*, a genetically tractable established model of neuronal connectivity. Interestingly, the neural network underpinning olfactory perception and odor naming is compromised early in AD[16]. Each mouse olfactory sensory neuron (OSN) expresses a single olfactory receptor (OR), choosing from over one thousand OR genes[17]. Each OR gene can be modified to express marker proteins or disease genes in a defined OSN cell type with exquisite specificity. To a first approximation, this circuit is organized as over 1000 parallel channels defined by OR proteins, which govern the response properties to odors[18] and the sites of axon projection on the surface of the olfactory bulb[19, 20]. Collectively, these OR-dictated projection loci form a stereotyped map. We find that overexpression of the Swedish mutation of human APP (hAPPsw), which causes early onset AD[21], disrupts the connectivity of OSNs, reduces activity-dependent gene expression in second-order olfactory neurons, and compromises olfactory acuity. These findings are not present in control mouse lines that overexpress wild type hAPP or M671V human APP (hAPPmv). Moreover, expression of Aβ40 or Aβ42 restricted to the olfactory epithelium also disturbs OSN axon targeting. These results indicate that human Aβ induces axon dysfunction *in vivo* in the absence of amyloid plaques.

Results

OSN Axons Mistarget in Mice Overexpressing hAPPsw

Axons of OSNs expressing the same OR innervate discrete glomeruli on the surface of the olfactory bulb (Fig. 1a). The naturally occurring hAPPsw (K670N, M671L) augments cleavage by the β-secretase thereby increasing Aβ production (Fig. 1b)[22]. We bred Tg2576 mice[22], which overexpress hAPPsw throughout the brain, including OSNs in the olfactory epithelium (Supplementary Figure S1) with a mouse line in which the *P2* OR gene was modified to also express GFP[20]. In control animals, a single glomerulus predominantly received fluorescent fibers in each bulb hemisphere. (Fig. 1c – d). By contrast, in littermate animals overexpressing hAPPsw, P2 axon projections terminate within multiple glomeruli per half bulb (Fig. 1e – f).

To confirm this phenotype, we examined a distinct subpopulation of OSNs expressing a different olfactory receptor, MOR28. In control mice, axons labeled with an antibody against MOR28[23] projected to only one glomerulus per half bulb (Fig. 1g – h). However, in Tg2576 mice multiple adjacent glomeruli per half olfactory bulb received MOR28-labelled fibers (Fig. 1i – j). This phenotype was observed in both males and females, and at ages ranging from 10 days to 12 months. Thus, mistargeting of axons in the olfactory system occurs before plaque deposition in the olfactory bulbs of Tg2576 mice (Fig. 1k – n).

Intact Targeting in Mice Overexpressing Wild type Human APP

In I5 mice overexpressing the wild type human APP gene (hAPPwt)[9], immunostaining of the olfactory epithelium revealed robust expression of hAPPwt in OSNs (Figure 2a – b). We

bred the I5 mouse line with a line in which the *P2* OR gene was modified to also express the fusion protein mouse tau-β-galactoside (tauLacZ)[20]. Immunostaining of the olfactory bulb using an anti-LacZ antibody did not reveal differences in targeting of axons of OSNs expressing P2 (Fig. 2c – d). Similiarly, the fidelity of targeting of axons of OSNs expressing MOR28 was also preserved (Fig. 2e – f) relative to littermate controls. These preserved axon projection patterns suggest that overexpression of the hAPPsw allele alters connectivity of this neural circuit.

Selective Expression of hAPPsw in OSNs Alters Connectivity

To determine whether expression of hAPPsw exclusively in OSNs was sufficient to cause OSN axon mistargeting, we generated transgenic mouse lines that coexpress hAPPsw and the axonal marker human placental alkaline phosphatase (PLAP) in a conditional manner using the tetracycline transcriptional activator (TTA)/*TetO* system[24]. These transgenic lines were crossed with a mouse line where the olfactory marker protein (OMP) gene was modified to coexpress TTA (Fig. 3a)[25]. Immunohistochemical analysis of the olfactory epithelium of compound heterozygote mice demonstrated that a subset of the OSNs express hAPPsw (Fig. 3b – c). Immunostaining of the olfactory bulb indicated that OSNs expressing PLAP project broadly to the glomeruli of the olfactory bulb (Fig. 3d – e). Overall, approximately 12% (319/2653) of OSNs expressed the transgene products hAPPsw and PLAP, except in the very lateral region where the expression was markedly reduced, 1.4% (28/2017). The proportion of expression in the M71-defined subpopulation was 18.4% (28 hAPP+/152 OSNs), but the expression of hAPPsw in the lateral OSNs expressing MOR28 was 0.19% (5 hAPP+/2604 OSNs). Importantly, we do not observe a shift in the pattern of expression of ORs over the olfactory epithelium. This mouse line expressing hAPPsw and PLAP was termed CORMAP (Conditional, Olfactory Sensory Neuron Restricted Mosaic expression of APPsw and PLAP).

Immunostaining of CORMAP mice bearing a modified P2 gene also expressing the tau-LacZ fusion protein[20] revealed multiple glomeruli receiving fibers labeled with LacZ, which was significantly different from immunostaining littermate P2/tau-LacZ mice expressing only the TTA transcription factor alone (Fig. 3f – h; $p < 0.001$; two-tailed t test; $n = 15$ (control); $n = 18$ (CORMAP)). Similarly, crossing CORMAP mice with a mouse line with a modified M71 gene also expressing the tau-LacZ fusion protein[26] revealed multiple glomeruli receiving LacZ fibers per half bulb (Fig. 3i – k; $p < 0.04$; two tailed t test; $n = 17$ (control); $n = 12$ (CORMAP)). OSNs expressing MOR28 predominantly targeted one glomerulus per half bulb in CORMAP mice and control littermates (Fig. 3l – n); the intact targeting likely reflects the scant transgene expression in that region of the epithelium. Overall the axon guidance phenotypes were similar to those observed in Tg2576, indicating that restricted expression of hAPPsw to OSNs is sufficient to disrupt their axon targeting.

Selective Expression of hAPPmv in OSNs Maintains Connectivity

Since hAPPsw facilitates production of Aβ, we generated transgenic mouse lines that coexpresses M671V human APP (hAPPmv) (Fig. 1b), a hAPP isoform that impairs Aβ production[12], and the axonal marker mCherry in a conditional manner as described above (Fig. 4a). Similarly, a subset of medial OSNs (17.6%; 239/1366) expressed hAPPmv and mCherry (Fig. 4b – c), and smaller subset of lateral OSNs (4.7%; 37/782) expressed the transgene. OSNs expressing mCherry projected broadly to the glomeruli in the olfactory bulb (Fig. 4d – e). The proportion of transgene expression in the MOR28-defined subpopulation mirrored the ambient density of the lateral epithelium (4.6%; 26 hAPP+/568 OSNs). Moreover, we did not observe a shift in the pattern of expression of ORs over the olfactory epithelium. This mouse line expressing hAPPmv and mcherry was termed

CORMAC (Conditional, Olfactory Sensory Neuron Restricted Mosaic expression of APPmv and mCherry).

The number of glomeruli targeted by OSNs coexpressing P2 and tau-LacZ in CORMAC mice was similar to control littermates (Fig. 4f – h). Similarly, the distribution of targeted glomeruli by M71-expressing OSNs did not differ between CORMAC mice and control littermates (Fig. 4i – k). Moreover, predominantly one glomerulus per half bulb was labeled with an antibody against MOR28 in both hAPPmv and control littermates (Fig. 4l – n). In summary, the patterns of connectivity of OSNs in CORMAC mice were preserved, thus, demonstrating the specificity of the hAPPsw phenotype.

A mouse line overexpressing a synthetic APP isoform (mouse/human chimeric protein with Swedish and Indiana mutations) was recently reported to generate high levels of human Aβ, which in turn caused accelerated OSN death[27]. In our study, levels of activated caspase 3 and the density of OSN subpopulations in Tg2576, CORMAP, or CORMAC lines were not significantly different from control littermates (Supplementary Fig. S2).

Olfactory Deficits Correlate with Altered Connectivity

The OSN-specific restricted expression of hAPP isoforms in both CORMAP and CORMAC lines affords the opportunity to determine the functional consequence of these connectivity deficits using odor-evoked behavioral assays without the potential confounds that central neural circuits may be affected by hAPP expression. We assessed olfactory function in these lines using two paradigms. The response to 2,3,5-trimethyl-3-thiazoline (TMT), an odorant isolated from fox feces with an innate aversive response to mice, was monitored (Fig. 5a)[28]. CORMAP, but not CORMAC, mice spent significantly more time within region of the arena where TMT was present (Fig. 5b – c). Moreover, in an olfactory assay monitoring appetitive behavior [29], food restricted CORMAP mice took significantly more time to find food buried under mouse bedding relative to littermate controls (Fig. 5d – e). Together, these olfactory assays indicate that compromised olfactory function correlates with alterations in structural connectivity of the peripheral olfactory neural circuit.

Reduced Expression of Activity-Dependent Gene Products

To confirm that the functional responses of OSNs was compromised in the CORMAP line, we quantified tyrosine hydroxylase (TH) expression by periglomerular dopaminergic neurons as a surrogate marker of OSN input activity[30]. Statistically significant reductions in levels of the TH signal were measured in the glomerular layer of CORMAP mice relative to wild type littermates (Fig. 6a – c; $p < 0.01$; two-tailed t test; $n = 5$ mice per genotype) that had been housed in the same cage. In addition, we quantified the expression of the immediate early gene *Arc* in periglomerular and tufted neurons of CORMAP mice relative to littermate controls. We observe a significant reduction in the number of neurons expressing *Arc* (Fig. 6d – f; $p < 0.01$; two-tailed t test; $n = 60 – 100$ per genotype). Since periglomerular and tufted neurons in the olfactory bulbs of CORMAP mice do not express hAPPsw, we interpret these reduced levels of TH and *Arc* as reflecting reduced input from OSNs.

Expression Aβ40 or Aβ42 Disturbs OSN Axon Targeting

The specificity of the hAPPsw phenotype implies that a BACE1 cleavage product of APP mediates axon dysfunction of OSNs. To determine whether the expression of human Aβ disrupts axon targeting of OSNs, we transduced the olfactory epithelia of mice with AAV expressing either the Bri-Aβ40 fusion protein or the Bri-Aβ42 fusion protein, which are cleaved sequentially by furin to secrete the human Aβ40 or Aβ42 peptide, respectively[31]. We instilled one naris of M71/tauLacZ mice with AAV8 expressing either Bri-Aβ40 or Bri-

Aβ42. The uninfected side served as a control. After 12 weeks, examination of M71-expressing OSNs revealed disturbed axon targeting on the infected side compared with the non-infected side (Fig. 7a – c). In control experiments, infection of AAV8 expressing GFP in one naris did not disturb M71 axon targeting (data not shown). Immunostaining of the olfactory epithelia from infected mice using the anti- human APP and Aβ antibody 6E10 revealed expression in the superficial layers of the olfactory epithelium. The cells expressing human Aβ40 costained with a marker for non-neuronal sustentacular cells (Supplementary Fig. S3a – d). Similarly, the infected side with Bri-Aβ42 expressing virus also caused axon mistargeting of M71-expressing axons (Fig. 7d – f). Of note, immunostaining of both the infected olfactory epithelium and the ipsilateral olfactory bulb with 6E10 did not reveal evidence of amyloid deposition (Supplementary Fig. S3e); moreover, formic acid extraction of the olfactory bulbs from the Bri-Aβ42 infected mice followed by ELISA did not detect Aβ42 (data not shown). These data support an extracellular mechanism of action of Aβ (that is likely to be soluble) to disturb axon targeting of OSNs. We cannot exclude the possibility that other cleavage products of APP contribute to the hAPPsw phenotype.

DISCUSSION

The increasing awareness of the susceptibility of olfactory acuity in people with prodromal neurodegenerative disease, relative to other sensory modalities, and our deeper understanding of the physiology underlying olfactory perception[32, 33] have made the olfactory neural network in animals a more widely used model to investigate mechanisms of neurodegenerative disease[34, 35]. The amenability of the mouse peripheral olfactory neural circuit to genetic, imaging, and behavioral characterization renders it a powerful model system to elucidate the actions of disease proteins[16, 27]. One of the unique aspects of this neural circuit is the continuous renewal of OSNs in adults[36], necessitating precise axon targeting throughout its lifetime to maintain the integrity of the circuit. We exploit this physiologic structural plasticity to visualize dysfunction caused by the expression of genes that cause neurologic disease. Here, we report that expression of the Swedish mutation of human APP in mice *in vivo* alters the connectivity and function of the peripheral olfactory neural circuit in the absence of plaques.

Our initial observation of this axon guidance phenotype occurred in well characterized lines that overexpress hAPPsw throughout the brain. Taking advantage of methodology to specifically express genes in the peripheral olfactory neural circuit[37], we generated and examined two lines of mice that overexpress human APP alleles exclusively in the presynaptic neurons of this circuit. Aβ production is facilitated in one line that expresses hAPPsw and impeded in the other line that expresses hAPPmv[12]. Overproduction of hAPPsw in the presynaptic neurons was sufficient to perturb the structural connectivity of the peripheral olfactory neural circuit. The absence of a phenotype in the hAPPmv line corroborated our findings in the mouse line overexpressing the wild type form of hAPP. Together with preserved fidelity of axon targeting in the I5 line overexpressing wild type hAPP throughout the brain, these important controls indicate that overexpression of human APP is not sufficient to alter OSN axonal connectivity. Rather, our findings suggest that products of BACE1-mediated cleavage of APP critically modulate neuronal function — in congruence with results from studies in hippocampal slices[13, 15, 38], in induced human neurons derived from skin fibroblasts[39] and studies of BACE1 heterozygous and null mice[40].

We postulate that Aβ is the BACE1 cleavage product of APP involved in mediating the connectivity phenotype. The presence of the connectivity phenotype in mice expressing hAPPsw, but not in the I5 line expressing hAPPwt and not in the CORMAC line expressing hAPPmv, supports this hypothesis. Moreover, expression of human Aβ40 or human Aβ42 in

the olfactory epithelium using a viral vector delivered intranasally phenocopies the alteration in the projection map of OSN axons. Since we observe these axon targeting deficits in young mice prior to the onset of plaques in the broadly expressing lines and since we do not observe amyloid plaques in lines that overexpress hAPP isoforms exclusively in OSNs or in the virally-infected mice, this novel axonal phenotype is independent of amyloid plaque deposition. This phenotype is unlikely to be caused by an in utero anomaly since we can induce it in adult control mice by intranasal expression of Aβ40 or Aβ42. Together, these data are consistent with a model that soluble Aβ triggers axonal dysfunction in the absence of amyloid plaques *in vivo*, although we cannot disprove that insoluble Aβ could also cause similar changes.

In addition to altering structural connectivity, expression of hAPPsw exclusively in OSNs has functional consequences as indicated by two lines of evidence. First, relative to control littermates or CORMAC mice, CORMAP mice exhibit significant reductions in olfactory acuity in two distinct behavioral paradigms, one paradigm employing an odor that evokes an aversive response while the other paradigm employs an odor that evokes an appetitive response. We interpret these olfactory-mediated behavioral responses as reflecting the function of the peripheral olfactory neural circuit in CORMAP and CORMAC lines — an interpretation afforded by the restricted expression pattern of hAPPsw and hAPPmv, respectively. Deficits in an odor habituation paradigm have been reported in Tg2576 mice at ages 6 - 7 months that correlated with amyloid plaque deposition[34]. By contrast, the behavioral phenotype of CORMAP mice is detectable at 3 to 5 months of age and is independent of amyloid plaques. Secondly, the expression of two independent activity-dependent markers in postsynaptic neurons in the olfactory bulb were significantly reduced in CORMAP mice relative to littermate controls. The magnitude of reduction of these activity-dependent markers (approx. 25%) exceeds the frequency of expression of hAPPsw in mature OSNs (approx. 12%). This disproportional response in the functional data raises the possibility that hAPPsw may be acting in a non-cell autonomous manner, as seen in studies in hippocampal slices by Malinow's laboratory[13, 38]. Our attempts to determine whether a non-cell autonomous mechanism underlies the structural connectivity phenotype in the CORMAP line have not been conclusive to date. Future studies employing expression of hAPP isoforms by specific OR promotors are aimed to address this question directly.

Our data illustrate a detrimental effect of heightened Aβ levels on a neural circuit in the absence of plaques. The CORMAP line offers a quantifiable outcome of the actions of hAPPsw, and likely Aβ, which is distinct from amyloid plaque production and that could be utilized to assess therapies targeting aberrant neural plasticity due to Aβ. While olfactory deficits have been shown in patients with prodromal and mild Alzheimer's disease, demonstration of alterations in the map of OSN projections in the human olfactory bulb in AD is necessary to postulate that the CORMAP mouse is a model for the disease. Increasing evidence indicates that Aβ levels rise after neuronal injury by increased expression of APP and/or BACE1[41]. Established risk factors for late onset AD, e.g. head trauma and vascular insults, result in elevated Aβ production[42]. Further delineation of the mechanism of action of human Aβ in this model system may provide insight into neural circuit and network dysfunction in the long, preclinical stage of Alzheimer's disease.

Methods

Animals

All experiments were in accordance with protocols approved by the Institutional Animal Care and Use Committee of Massachusetts General Hospital. Tg2576 mice overexpressing hAPPsw[22] were obtained from Taconic Farms (Hudson, NY). I5 hAPPwt mice[9], and M71-

ires-tauLacZ were obtained from Jackson Labs (Bar Harbor, ME). P2-ires-GFP[20] and P2-ires-tauLacZ[43] mice were a gift from Richard Axel.

Generation and Characterization of CORMAP and CORMAC Mice

Transgenic constructs were generated using the hAPPsw695 cDNA, ires-PLAP[44] and pBSRV[37] which contained the tetO sequence followed by an artificial intron and splice site, the Pac site, and an SV40 polyadenylation signal. For the CORMAC mice, the hAPPsw695 (K670N; M671L) cDNA was mutated to the mv genotype (M671V) by PCR mutagenesis (Stratagene) and confirmed by sequencing. A DNA fragment encoding ires-mcherry was isolated and the hAPPmv-ires-mcherry fragment was cloned and injected. The founder mouse was crossed with OMP-ires-tTA mice[25]. Compound heterozygote mice of the founders for the CORMAP line expressed hAPPsw and PLAP in approximately 12% of OSNs and not elsewhere in the brain. This line was backcrossed into C57/BL6 for six generations. Compound heterozygote mice of a founder for the CORMAC line expressed hAPPsw and mCherry in approximately 18% of OSNs and not elsewhere in the brain. This line was backcrossed into C57/BL6 for six generations. The ages of mice used in this study ranged from 3 weeks to 1 year.

Immunohistochemistry

Standard procedures were used as previously described[45]. The mice were anesthetized with an intraperitoneal injection of 3,3,3-tribromoethanol (1.25% in PBS 30 μL/g body weight). Following thoracotomy, intracardiac perfusion with 10 mL of PBS (pH 7.4) was performed. For anti-GFP and anti-LacZ immunostaining, the mice were subsequently perfused with 2% paraformaldehyde in PBS (pH 7.4). The olfactory turbinates and olfactory bulbs were dissected intact, incubated in 30% sucrose in PBS at 4 °C overnight, and embedded in OCT (Sakura) or M1 (Shandon) in a dry ice/ethanol bath. Twenty μm coronal sections were cut on a cryostat (Microm) and collected on SuperFrost slides (Fisher). For immunostaining using the MOR28 and M71 antibodies, the sections were post-fixed with 1% paraformaldehyde in PBS for 8 min. at room temperature. All sections were washed three times in PBS for 10 min., permeabilized in 0.1% Triton X-100 in PBS (PT) for 30 min. at room temperature, blocked in 5% heat-inactivated horse serum in PT (PTS) for 1 h at room temperature, incubated with primary antibody in PTS under a Hybrislip (Invitrogen) overnight in a humidified chamber at 4 °C, washed three times with PT for 10 min, blocked with PTS for 30 min at room temperature, incubated with a fluorescent-conjugated secondary antibody in PTS with DAPI (Invitrogen, 1:1000) for 2 h at room temperature, washed briefly in PBS, and Vectashield was applied to each slide and coverslipped. Slides were analyzed using a Zeiss LSM-510 confocal microscope or a Leica confocal microscope and analyzed using ImageJ (NIH).

Primary antibodies included rabbit anti-GFP (Molecular Probes; 1:1000), sheep anti-GFP (Biogenesis; 1:1000), rabbit anti-LacZ (Cappel; 1;1000), rabbit anti-APP (6900; Zymed; 1;1000), mouse anti-human APP and Aβ (4G8 and 6E10; Covance; 1:1000); rabbit anti-MOR28 (1:3000) [23] guinea pig anti-M71 (1:1000)[23], rabbit anti-activated caspase 3 (Cell Signaling, 1:500), rabbit anti-TROMA (Molecular Probes; 1:10), and mouse anti-tyrosine hydroxylase (Millipore; 1:500). Secondary antibodies were Alexa 488-conjugated donkey anti-rabbit Ig (Molecular Probes; 1:500), Alexa 488-conjugated donkey anti-sheep Ig (Molecular Probes; 1: 500), Cy3-conjugated donkey anti-guinea pig Ig (Jackson Immunoresearch; 1: 500), Cy3-conjugated rat anti-mouse Ig (Jackson Immunoresearch; 1:500).

In situ hybridization

Twenty μm thick fresh frozen tissue sections were placed on Superfrost slides (Fisher Scientific). The sections were dried for 45 minutes at room temperature before fixing with 4% paraformaldehyde for 15 minutes, and washed 3x in 1x DEPC-treated PBS containing 1mM $MgCl_2$. Slides were then immersed in a solution containing 270 mL of DEPC treated water, 30mL of 1M triethanolamine and 750 μL of 95% acetic anhydride for 10 minutes, and subsequently washed 3x in 1x DEPC-treated PBS containing 1mM MgCl2. Slides were then blocked for 2 hours with hyridization buffer: 0.1% Tween20, 50% formamide, 5x SSC, 5x Denhardts, 5mM EDTA, 10mM NaH2PO4 at pH. 8.0, 50mM Tris pH 8.0, 250 μg/mL salmon sperm DNA, 100 μgram/mL tRNA, 100 μg/mL yeast RNA. Slides were dabbed dry and *Arc* antisense RNA probes[46] (100 μg/mL), preheated for 5 minutes at 80 degrees and cooled on ice for 2 minutes, were applied to the slides and sealed in a humidified chamber at 65 overnight. After 18 hrs the slides were washed at 65 degrees C in 3x in 5xSSC for 15 min., and then 3x with 0.2x SSC for 20 min. After blocking in 1x in situ hybridization blocking solution (Roche) for 1 hour. Slides were dabbed dry and a sheep antibody recognizing digoxetin (1:3000, Roche) was applied overnight. The next day the RNA probe was detected using the HNPP fluorescent detection kit (Roche) or BCIP/NBT (Promega).

Whole mount

Whole mount analyses were performed as previously described[47]. Briefly, mice harboring the P2-ires-GFP allele were anesthesized as described above. The skull was dissected and then divided sagittally and the dura was removed from the medial surface of each olfactory bulb. Each whole mount was placed in PBS with 2 mM $MgCl_2$ and then imaged using a Leica confocal imaging system. Preparation and staining of olfactory bulbs expressing tau-LacZ was performed as previously described[20].

AAV infection

AAV was introduced intranasally in one naris of 2 month old M71-ires-tauLacZ mice (Bri-Aβ40) or control mice (Bri-Aβ42) by diluting 2.5 μL of AAV8 virus with 57.5 μL of 2% methylcellulose in PBS (1% final concentration; 5×10^{12} pfus) as previously described[48]. Analysis by immunohistochemistry and whole mount preparation occurred 90 days after infection.

Behavior

The TMT assay was derived from the curtain assay[28]. Briefly, the experiment was performed in the dark during the nocturnal phase of the day. The behavioral arena (Fig. 4a) was placed in a chemical hood. Mice (age range 3 – 5 m) were habituated to the arena for 3 × 10 min with blank filter papers. After 7 min. of the third habituation, the filter papers were swapped with identical filter papers with 20 μL of water or TMT, respectively. The remaining three minutes were videorecorded and scored in a blinded fashion. One-way analysis of variance and unpaired t-tests were used to analyze the data.

The hidden food assay was derived from similar assays previously described[29, 49]. The mice (age ≥ 3 – 9 m) were food restricted for 24 h and then habituated in an 82 cm × 63 cm × 18 cm arena with 2 cm autoclaved mouse bedding for 5 min. Then they are returned to their home cage for 30 min. Each animal was placed back in the arena with fresh autoclaved bedding covering 1 g of ground food pellet placed in one specific location. The trial was analyzed in real time using a stopwatch until the food was ingested. The experimenters recording the latency to eat the food were blinded to the genotype. The results of between two experimenters was not significantly different. Each animal was tested once.

Statistical Analysis One-way analysis of variance and unpaired t-tests were performed using SAS, Microsoft Excel, or Apple Numbers and results are presented as mean ± s.e.m.

Supplementary Material

Refer to Web version on PubMed Central for supplementary material.

Acknowledgments

We thank R. Axel, S. D. Liberles, and A. D. Albers for insightful comments, A. Nemes, M. Mendelssohn, and J. Kirkland for generating the CORMAP mouse lines, L. Wu for generating the CORMAC mouse lines, C. M. William for the *Arc* in situ probe, H. Brown, N. Bevins, H. Wei, N. Propp, M. Glinka, M. Hood, and Z. Doctor for excellent technical assistance, M. Arimon for performing the ELISA, and G. Sun for statistical analyses. This work was supported by the AFAR-Ellison Foundation (awarded to L.C.), the NIH (K08 DC04807 and DP2 OD006662, awarded to M.W.A.; P30AG036449, awarded to B.T.H.), and the Rappaport Foundation (awarded to M.W.A.).

References

1. Palop JJ, Mucke L. Amyloid-beta-induced neuronal dysfunction in Alzheimer's disease: from synapses toward neural networks. Nat Neurosci. 2010; 13:812–818. [PubMed: 20581818]
2. Sperling RA, et al. Amyloid deposition is associated with impaired default network function in older persons without dementia. Neuron. 2009; 63:178–188. [PubMed: 19640477]
3. Hedden T, et al. Disruption of functional connectivity in clinically normal older adults harboring amyloid burden. J Neurosci. 2009; 29:12686–12694. [PubMed: 19812343]
4. Jack CR Jr. et al. Serial PIB and MRI in normal, mild cognitive impairment and Alzheimer's disease: implications for sequence of pathological events in Alzheimer's disease. Brain. 2009; 132:1355–1365. [PubMed: 19339253]
5. Sheng M, Sabatini BL, Sudhof TC. Synapses and Alzheimer's Disease. Cold Spring Harb Perspect Biol. 2012
6. Ashe KH, Zahs KR. Probing the biology of Alzheimer's disease in mice. Neuron. 2010; 66:631–645. [PubMed: 20547123]
7. Koffie RM, et al. Oligomeric amyloid beta associates with postsynaptic densities and correlates with excitatory synapse loss near senile plaques. Proc Natl Acad Sci U S A. 2009; 106:4012–4017. [PubMed: 19228947]
8. Kuchibhotla KV, et al. Abeta plaques lead to aberrant regulation of calcium homeostasis in vivo resulting in structural and functional disruption of neuronal networks. Neuron. 2008; 59:214–225. [PubMed: 18667150]
9. Mucke L, et al. High-level neuronal expression of abeta 1-42 in wild-type human amyloid protein precursor transgenic mice: synaptotoxicity without plaque formation. J Neurosci. 2000; 20:4050–4058. [PubMed: 10818140]
10. Li S, et al. Soluble oligomers of amyloid Beta protein facilitate hippocampal long-term depression by disrupting neuronal glutamate uptake. Neuron. 2009; 62:788–801. [PubMed: 19555648]
11. Shankar GM, et al. Amyloid-beta protein dimers isolated directly from Alzheimer's brains impair synaptic plasticity and memory. Nat Med. 2008; 14:837–842. [PubMed: 18568035]
12. Citron M, Teplow DB, Selkoe DJ. Generation of amyloid beta protein from its precursor is sequence specific. Neuron. 1995; 14:661–670. [PubMed: 7695913]
13. Wei W, et al. Amyloid beta from axons and dendrites reduces local spine number and plasticity. Nat Neurosci. 2010; 13:190–196. [PubMed: 20037574]
14. Venkitaramani DV, et al. Beta-amyloid modulation of synaptic transmission and plasticity. J Neurosci. 2007; 27:11832–11837. [PubMed: 17978019]
15. Hsieh H, et al. AMPAR removal underlies Abeta-induced synaptic depression and dendritic spine loss. Neuron. 2006; 52:831–843. [PubMed: 17145504]
16. Albers MW, Tabert MH, Devanand DP. Olfactory dysfunction as a predictor of neurodegenerative disease. Curr Neurol Neurosci Rep. 2006; 6:379–386. [PubMed: 16928347]

17. Vassar R, et al. Topographic organization of sensory projections to the olfactory bulb. Cell. 1994; 79:981–991. [PubMed: 8001145]
18. Malnic B, Hirono J, Sato T, Buck LB. Combinatorial receptor codes for odors. Cell. 1999; 96:713–723. [PubMed: 10089886]
19. Feinstein P, Mombaerts P. A contextual model for axonal sorting into glomeruli in the mouse olfactory system. Cell. 2004; 117:817–831. [PubMed: 15186781]
20. Wang F, Nemes A, Mendelsohn M, Axel R. Odorant receptors govern the formation of a precise topographic map. Cell. 1998; 93:47–60. [PubMed: 9546391]
21. Mullan M, et al. A pathogenic mutation for probable Alzheimer's disease in the APP gene at the N-terminus of beta-amyloid. Nat Genet. 1992; 1:345–347. [PubMed: 1302033]
22. Hsiao K, et al. Correlative memory deficits, Abeta elevation, and amyloid plaques in transgenic mice. Science. 1996; 274:99–102. [PubMed: 8810256]
23. Barnea G, et al. Odorant receptors on axon termini in the brain. Science. 2004; 304:1468. [PubMed: 15178793]
24. Kistner A, et al. Doxycycline-mediated quantitative and tissue-specific control of gene expression in transgenic mice. Proc Natl Acad Sci U S A. 1996; 93:10933–10938. [PubMed: 8855286]
25. Yu CR, et al. Spontaneous neural activity is required for the establishment and maintenance of the olfactory sensory map. Neuron. 2004; 42:553–566. [PubMed: 15157418]
26. Feinstein P, Bozza T, Rodriguez I, Vassalli A, Mombaerts P. Axon guidance of mouse olfactory sensory neurons by odorant receptors and the beta2 adrenergic receptor. Cell. 2004; 117:833–846. [PubMed: 15186782]
27. Cheng N, Cai H, Belluscio L. In vivo olfactory model of APP-induced neurodegeneration reveals a reversible cell-autonomous function. J Neurosci. 2011; 31:13699–13704. [PubMed: 21957232]
28. Kobayakawa K, et al. Innate versus learned odour processing in the mouse olfactory bulb. Nature. 2007; 450:503–508. [PubMed: 17989651]
29. Fleming SM, et al. Olfactory deficits in mice overexpressing human wildtype alpha-synuclein. Eur J Neurosci. 2008; 28:247–256. [PubMed: 18702696]
30. Baker H. Unilateral, neonatal olfactory deprivation alters tyrosine hydroxylase expression but not aromatic amino acid decarboxylase or GABA immunoreactivity. Neuroscience. 1990; 36:761–771. [PubMed: 1700334]
31. Lawlor PA, et al. Novel rat Alzheimer's disease models based on AAV-mediated gene transfer to selectively increase hippocampal Abeta levels. Mol Neurodegener. 2007; 2:11. [PubMed: 17559680]
32. Gottfried JA. Central mechanisms of odour object perception. Nat Rev Neurosci. 2010; 11:628–641. [PubMed: 20700142]
33. Wilson DA, Sullivan RM. Cortical processing of odor objects. Neuron. 2011; 72:506–519. [PubMed: 22099455]
34. Wesson DW, Levy E, Nixon RA, Wilson DA. Olfactory dysfunction correlates with amyloid-beta burden in an Alzheimer's disease mouse model. J Neurosci. 2010; 30:505–514. [PubMed: 20071513]
35. Wesson DW, et al. Sensory network dysfunction, behavioral impairments, and their reversibility in an Alzheimer's beta-amyloidosis mouse model. J Neurosci. 2011; 31:15962–15971. [PubMed: 22049439]
36. Graziadei PP, Graziadei GA. Neurogenesis and neuron regeneration in the olfactory system of mammals. I. Morphological aspects of differentiation and structural organization of the olfactory sensory neurons. J Neurocytol. 1979; 8:1–18. [PubMed: 438867]
37. Gogos JA, Osborne J, Nemes A, Mendelsohn M, Axel R. Genetic ablation and restoration of the olfactory topographic map. Cell. 2000; 103:609–620. [PubMed: 11106731]
38. Kamenetz F, et al. APP processing and synaptic function. Neuron. 2003; 37:925–937. [PubMed: 12670422]
39. Qiang L, et al. Directed conversion of Alzheimer's disease patient skin fibroblasts into functional neurons. Cell. 2011; 146:359–371. [PubMed: 21816272]

40. Cao L, Rickenbacher GT, Rodriguez S, Moulia TW, Albers MW. The precision of axon targeting of mouse olfactory sensory neurons requires the BACE1 protease. Sci. Rep. 2012; 2:1–8.
41. O'Connor T, et al. Phosphorylation of the translation initiation factor eIF2alpha increases BACE1 levels and promotes amyloidogenesis. Neuron. 2008; 60:988–1009. [PubMed: 19109907]
42. Reitz C, Brayne C, Mayeux R. Epidemiology of Alzheimer disease. Nat Rev Neurol. 2011; 7:137–152. [PubMed: 21304480]
43. Mombaerts P, et al. Visualizing an olfactory sensory map. Cell. 1996; 87:675–686. [PubMed: 8929536]
44. Shah NM, et al. Visualizing sexual dimorphism in the brain. Neuron. 2004; 43:313–319. [PubMed: 15294140]
45. Cao L, et al. Genetic modulation of BDNF signaling affects the outcome of axonal competition in vivo. Curr Biol. 2007; 17:911–921. [PubMed: 17493809]
46. William CM, et al. Synaptic plasticity defect following visual deprivation in Alzheimer's disease transgenic mice. J Neurosci. 2012 in press.
47. Shykind BM, et al. Gene switching and the stability of odorant receptor gene choice. Cell. 2004; 117:801–815. [PubMed: 15186780]
48. Gau P, Rodriguez S, De Leonardis C, Chen P, Lin DM. Air-assisted intranasal instillation enhances adenoviral delivery to the olfactory epithelium and respiratory tract. Gene Ther. 2011
49. Crawley, JN. What's Wrong With My Mouse?. Wiley-Liss; New York: 2000.

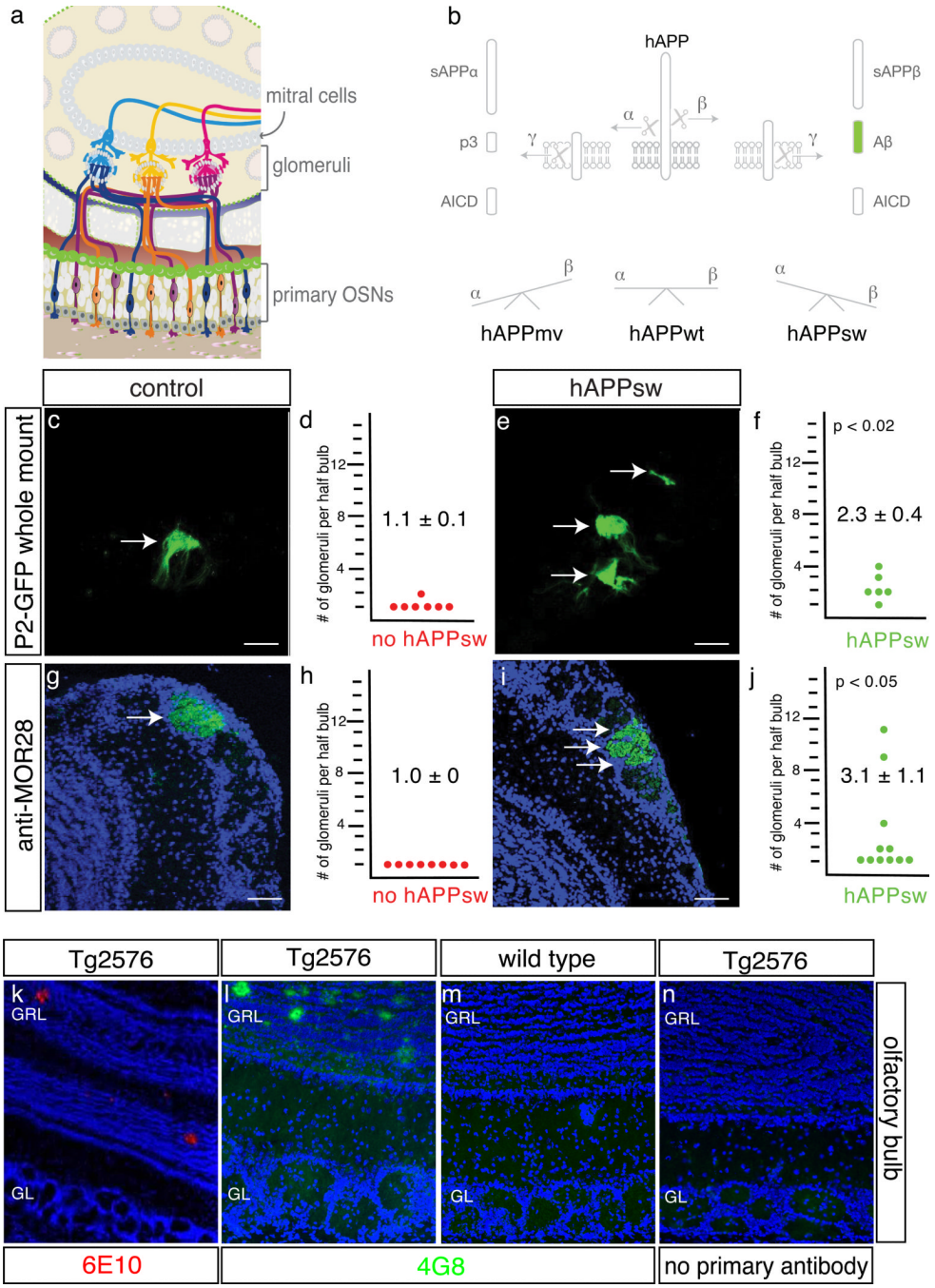

Figure 1. Aberrant OSN projections in transgenic mouse lines overexpressing hAPPsw

(a) Schematic representation of the anatomy of the peripheral olfactory neural circuit demonstrating that choice of olfactory receptor (OR) (depicted by color) dictates the projection target of its axon in the olfactory bulb. **(b)** Schematic representation of the protease cleavage pathways to generate Aβ and other fragments from hAPP. The mutation hAPPsw enhances flux through the β-secretase pathway and M671V human APP (hAPPmv) impairs flux through the β-secretase pathway. **(c–d)** Representative image of olfactory bulbs from P2-ires-GFP mice reveal a single glomerulus (indicated by arrow) per half bulb is targeted by axons containing GFP (each dot represents result per half bulb;). **(e–f)**

Representative image and quantification of olfactory bulbs from Tg2576 (panneuronal hAPPsw)/P2-ires-GFP mice reveal aberrant targeting of fibers containing GFP to multiple glomeruli (arrows) per half bulb ($p < 0.02$, two tailed t test; $n = 7$ (controls); $n = 6$ (Tg2576)). **(g–h)** Representative coronal section and quantification of olfactory bulbs from wild type mice immunostained with anti-MOR28 and TOTO-3 reveal targeting to a single glomerulus (arrow). **(i–j)** Representative coronal section and quantification of olfactory bulbs from Tg2576 hAPPsw mice immunostained with anti-MOR28 and TOTO-3 reveal aberrant targeting of MOR28 axons to multiple glomeruli (arrows) ($p < 0.05$, two tailed t test; $n = 8$ (controls); $n = 11$ (Tg2576)). Data presented as means ± s.e.m. **(k)** The olfactory bulb from a 13-month old Tg2576 mouse immunostained with 6E10 anti-APP antibody shows the presence of plaques in the granule cell layer (GR). No plaques are seen in the glomerular layer (GL). **(l–n)** The human-specific antibody 4G8 reveals expression of hAPPsw in the glomerular layer (GL) of Tg2576 (24 months old), but not in wild type mice **(m)** or when 4G8 is omitted from the Tg2576 tissue **(n)**. Plaques are seen in granule cell layer but not in the glomerular cell layers in the 24-month old Tg2576 mouse **(l)**. Scale bar = 100 μm.

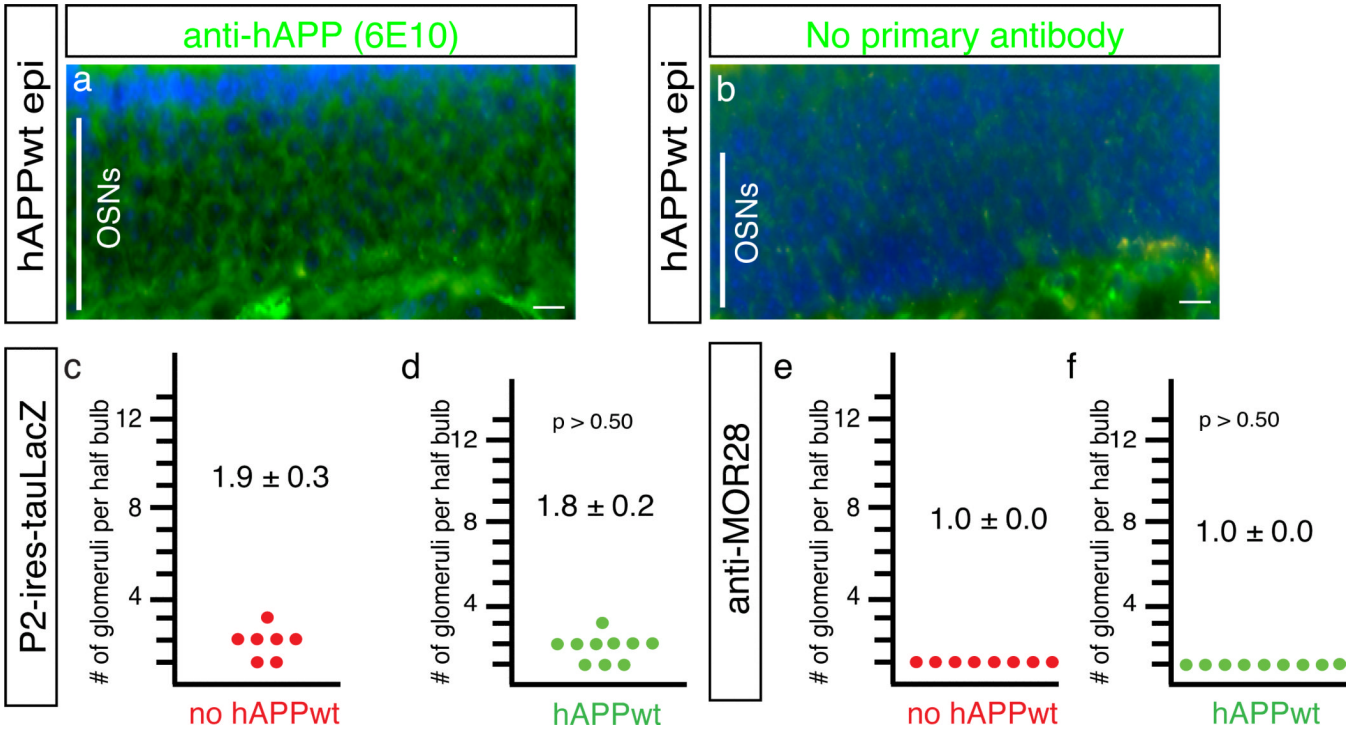

Figure 2. Preserved OSN projections in transgenic mouse lines overexpressing hAPPwt

(a–b) Olfactory epithelia harvested from 12 week old mice overexpressing the human APP protein driven by the PDGF β-promotor expressed APP as shown by immunostaining with anti-APP 6E10 **(a)** relative to a no primary antibody control **(b)**. Scale bar = 20 μm. **(c–d)** Quantification of olfactory bulbs from control one year old P2-ires-GFP mice and from I5 human wild type APP (hAPPwt)-overexpressing mice reveal targeting of fibers containing GFP to two glomeruli per half bulb in both lines ($p > 0.50$, two tailed t test; n = 7 (controls); n = 10 (I5)). **(e–f)** Quantification of olfactory bulbs from control mice and from I5 hAPPwt transgenic mice immunostained with anti-MOR28 reveal targeting to a single glomerulus ($p > 0.50$, two tailed t test; n = 8 (controls); n = 9 (I5)). Scale bar = 100 μm. Data presented as means ± s.e.m.

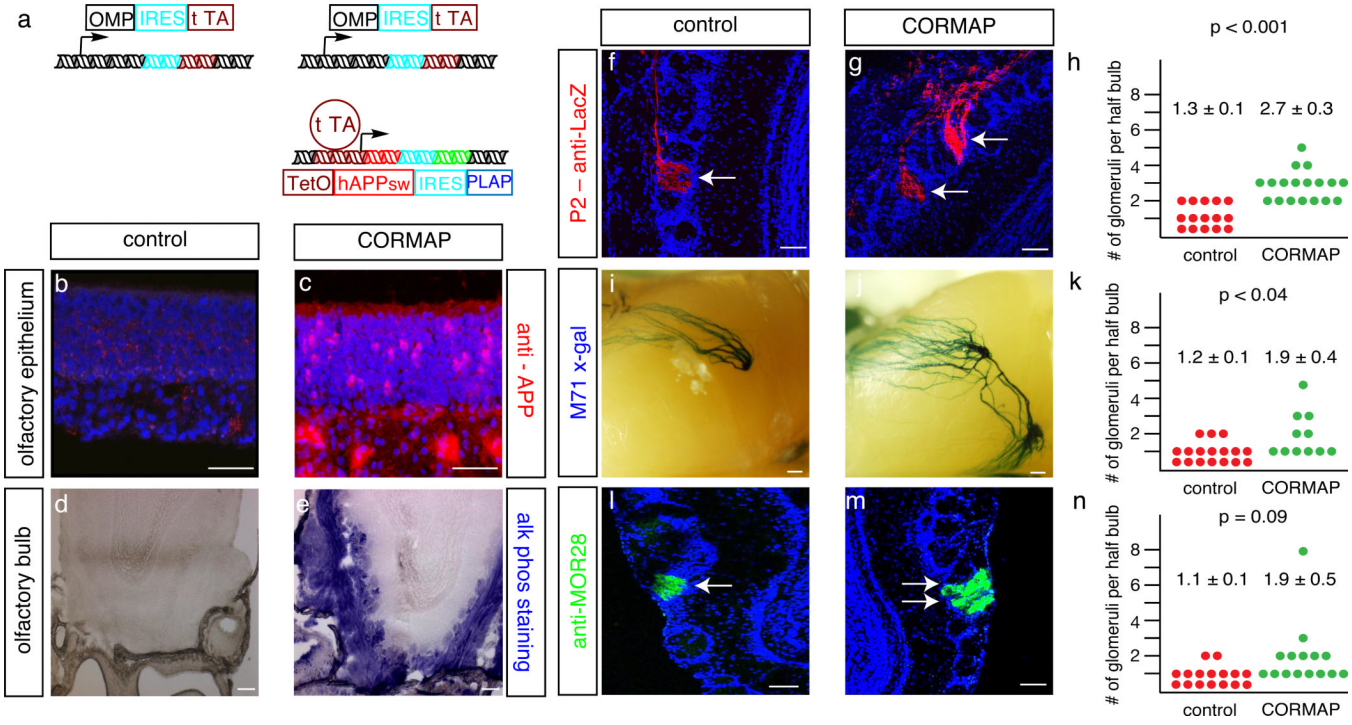

Figure 3. Characterization of CORMAP mice

(a) Schematic diagram of the *olfactory marker protein* (*OMP)* gene locus altered by homologous recombination to introduce the internal ribosomal entry sequence (IRES) and tetracycline transcriptional activator (TTA) (OMP-ivt) and the transgene encoding the operator sequence *TetO* followed by hAPPsw, IRES, and PLAP. **(b–c**) Coronal section of the medial olfactory epithelium from a control and a CORMAP mouse immunostained with an anti-APP antibody reveals background expression of the endogenous mouse APP in OSNs and approximately 12% of OSNs overexpress hAPPsw, respectively. **(d–e)** Coronal section of the olfactory bulb of a control and a CORMAP mouse colorimetrically stained for PLAP activity reveals that PLAP-labelled fibers target glomeruli in a stochastic pattern. **(f–h)** Representative images and quantification of olfactory bulbs from P2-ires-tauLacZ (tau-β-galactosidase fusion protein)/OMP-ivt and P2-ires-tauLacZ/CORMAP mice reveal targeting of LacZ-bearing neurons to one glomerulus (arrow) in control mice and targeting of LacZ-bearing axons to multiple glomeruli (arrows) in CORMAP mice (arrows identify glomeruli revealing P2-expressing fibers) ($p < 0.001$, two tailed t test; n = 15 (controls); n = 18 (CORMAP)). **(i–k)** Representative images and quantification of olfactory bulbs from M71-ires-tauLacZ/OMP-ivt and littermate M71-ires-tauLacZ/CORMAP mice reveal targeting of LacZ-bearing neurons to one glomerulus in controls and to multiple glomeruli in CORMAP mice with some fibers crossing between the lateral and medial projection loci. ($p < 0.04$, two tailed t test; n = 17 (controls); n = 11 (CORMAP)) **(l–n)** Representative images and quantification of olfactory bulbs from control and littermate CORMAP mice stained with anti-MOR28 antibody reveals MOR28-bearing axons targeting predominantly to a single glomerulus per half bulb in both lines ($p < 0.09$, two tailed t test; n = 16 (controls); n = 15 (CORMAP)). Scale bars = 100 μm, except for (i–j) where scale bar = 200 μm. Data presented as means ± s.e.m.

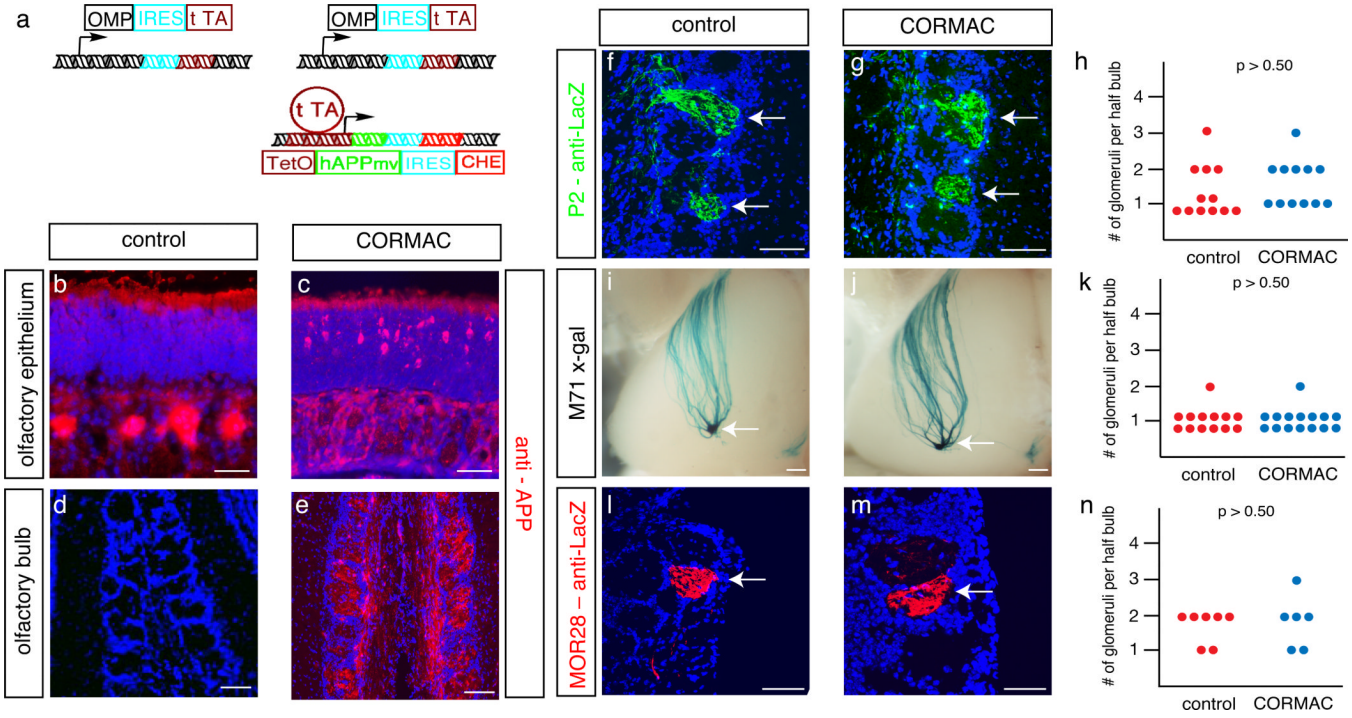

Figure 4. Characterization of CORMAC mice

(a) Schematic diagram of the *OMP* gene locus altered by homologous recombination to introduce the IRES and TTA(OMP-ivt) and the transgene encoding the operator sequence *TetO* followed by hAPPmv (hAPP M671V), IRES, and the mCherry (CHE). **(b–c)** Coronal section of the medial olfactory epithelium from control and CORMAC mice immunostained with an anti-APP antibody reveals background expression of the endogenous mouse APP in OSNs and approximately 18% of OSNs overexpress hAPPmv, respectively. **(d–e)** Coronal sections of olfactory bulbs from a control mouse and a CORMAC mouse reveal fibers containing mCherry target glomeruli in a stochastic pattern. **(f–h)** Representative images and quantification of olfactory bulbs from P2-ires-tauLacZ/OMP-ivt and P2-ires-tauLacZ/CORMAC mice reveal targeting of LacZ-bearing neurons to equal glomeruli (arrows) in both control and CORMAC mice. ($p > 0.50$, two tailed t test; n = 12 (controls); n = 12 (CORMAC)) **(i–k)** Representative images and quantification of olfactory bulbs from M71-ires-tauLacZ/OMP-ivt and littermate M71-ires-tauLacZ/CORMAC mice reveal targeting of LacZ-bearing neurons to one glomerulus in both control and CORMAC mice. ($p > 0.50$, two tailed t test; n = 13 (controls); n = 15 (CORMAC)) **(l–n)** Representative images and quantification of olfactory bulbs from MOR28-ires-tauLacZ/OMP-ivt and littermate MOR28-ires-tauLacZ/CORMAC mice reveal targeting of LacZ-bearing neurons to one glomerulus (arrow) in both control and CORMAC mice ($p > 0.50$, two tailed t test; n = 7 (controls); n = 6 (CORMAC)). Scale bars = 100 μm, except for (d-e, i–j) where scale bar = 200 μm.

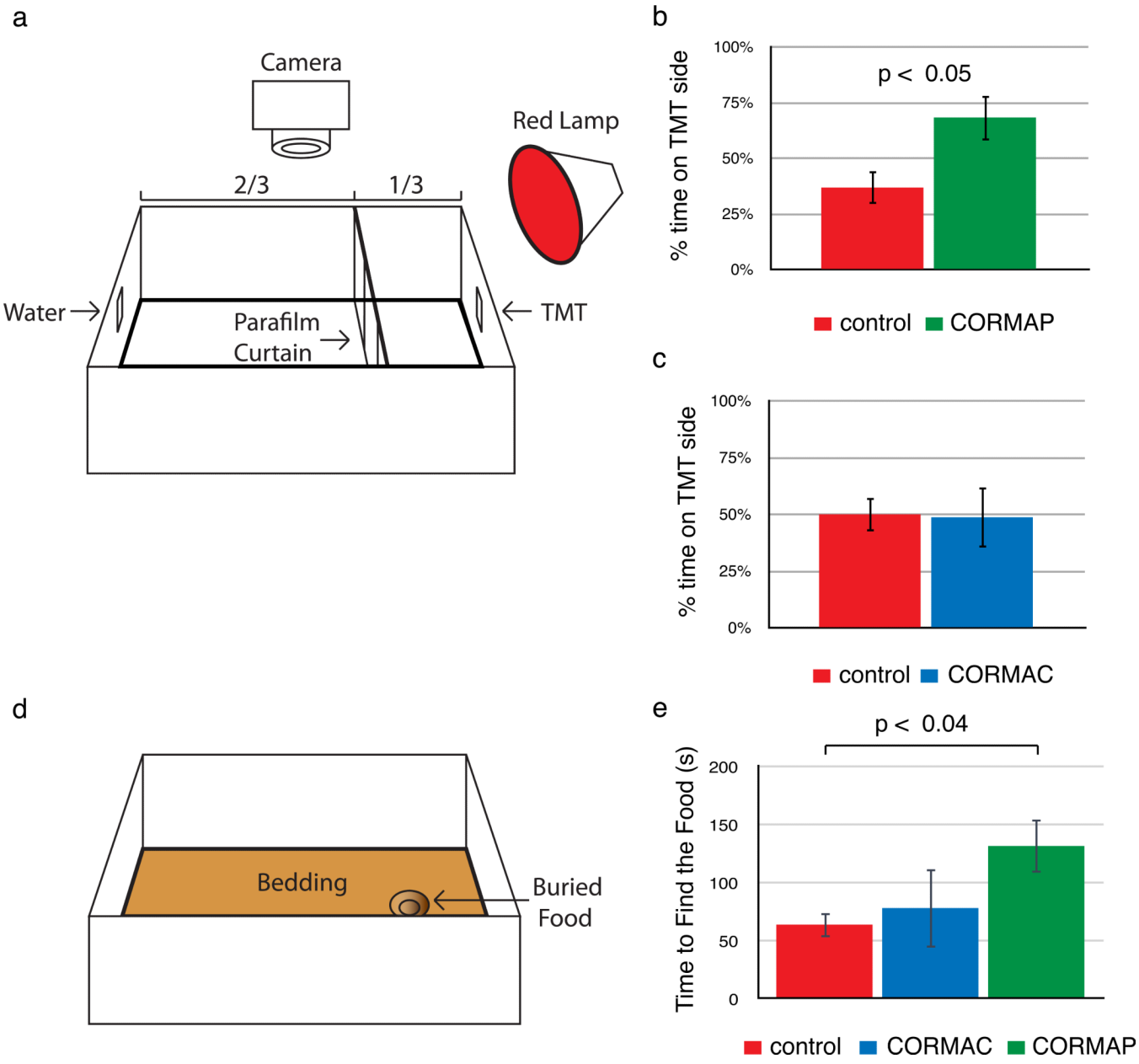

Figure 5. Olfactory behavioral deficit in the CORMAP mice but not CORMAC mice

(**a**) Schematic representation of the behavioral arena to assess the response to 2,3,5-trimethyl-3-thiazoline (TMT), an odor isolated from fox feces that triggers an innate aversion response in mice. (**b–c**) Percentage of time that each mouse spent in a compartment with the innately aversive odor TMT relative to a compartment with water for a 3 minute period. Relative to littermate controls, CORMAC (hAPPmv) but not CORMAP (hAPPsw) mice avoided TMT. ($p < 0.05$; one-way ANOVA; n = 5 pairs of littermate mice for each genotype with ages ranging from 3 to 5 months). (**d**) Schematic representation of the behavioral arena to find the buried food. (**e**) Graphical representation of time to find food for controls, CORMAC, and CORMAP mice. Relative to controls, CORMAP, but not CORMAC, required a significantly longer time to find the food ($p < 0.04$; one-way ANOVA; n = 4 (control), 3 (CORMAC), and 4 (CORMAP) with ages ranging from 3 to 6 months). Error bars = s.e.m.

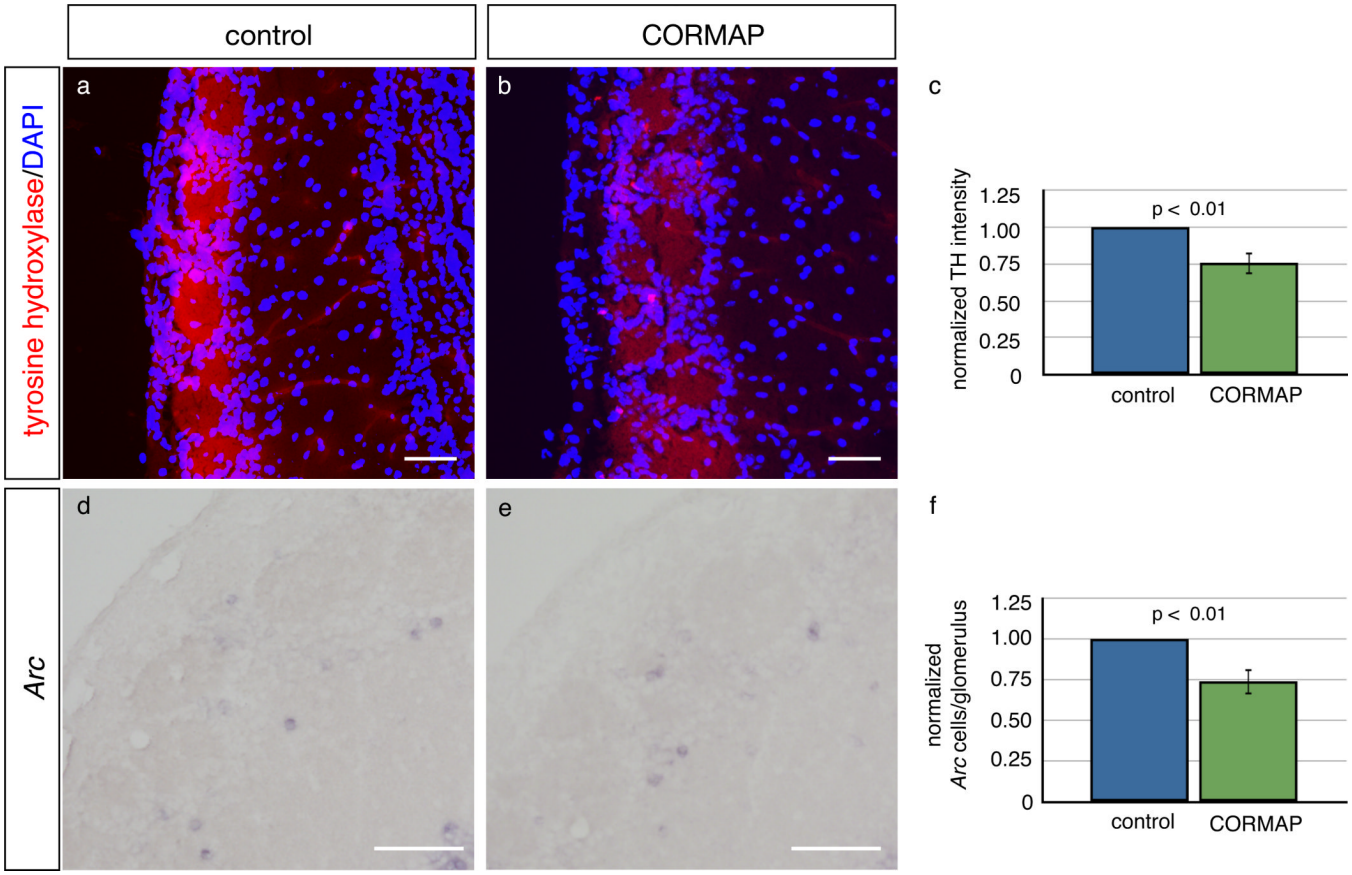

Figure 6. Reduced induction of OSN activity-dependent genes in CORMAP mice olfactory bulbs

(a) Representative image of olfactory bulbs from a control mouse immunostained with an antibody recognizing tyrosine hydroxylase (TH) (red) and a nuclear stain (blue). **(b)** Representative image of olfactory bulbs from a CORMAP mouse immunostained with an antibody recognizing TH (red) and a nuclear stain (blue). **(c)** Quantification of the intensity of TH staining in glomeruli of CORMAP (n = 5 bulbs) and littermate control mice (n = 5 bulbs) reveals a statistically significant difference ($p < 0.01$; two-tailed t test). **(d)** Representative image of an olfactory bulb from a control mouse following in situ hybridization with an antisense *Arc* probe. **(e)** Representative image of an olfactory bulb from a CORMAP mouse following in situ hybridization with an antisense *Arc* probe. **(f)** Quantification of number of periglomerular and tufted neurons expressing *Arc* in matched regions of the olfactory bulbs from CORMAP (n = 5) and littermate control mice (n = 5) reveals a significant difference ($p < 0.01$; two-tailed t test; n = 60 – 100 per genotype). Scale bar = 100 μm. Error bars = s.e.m.

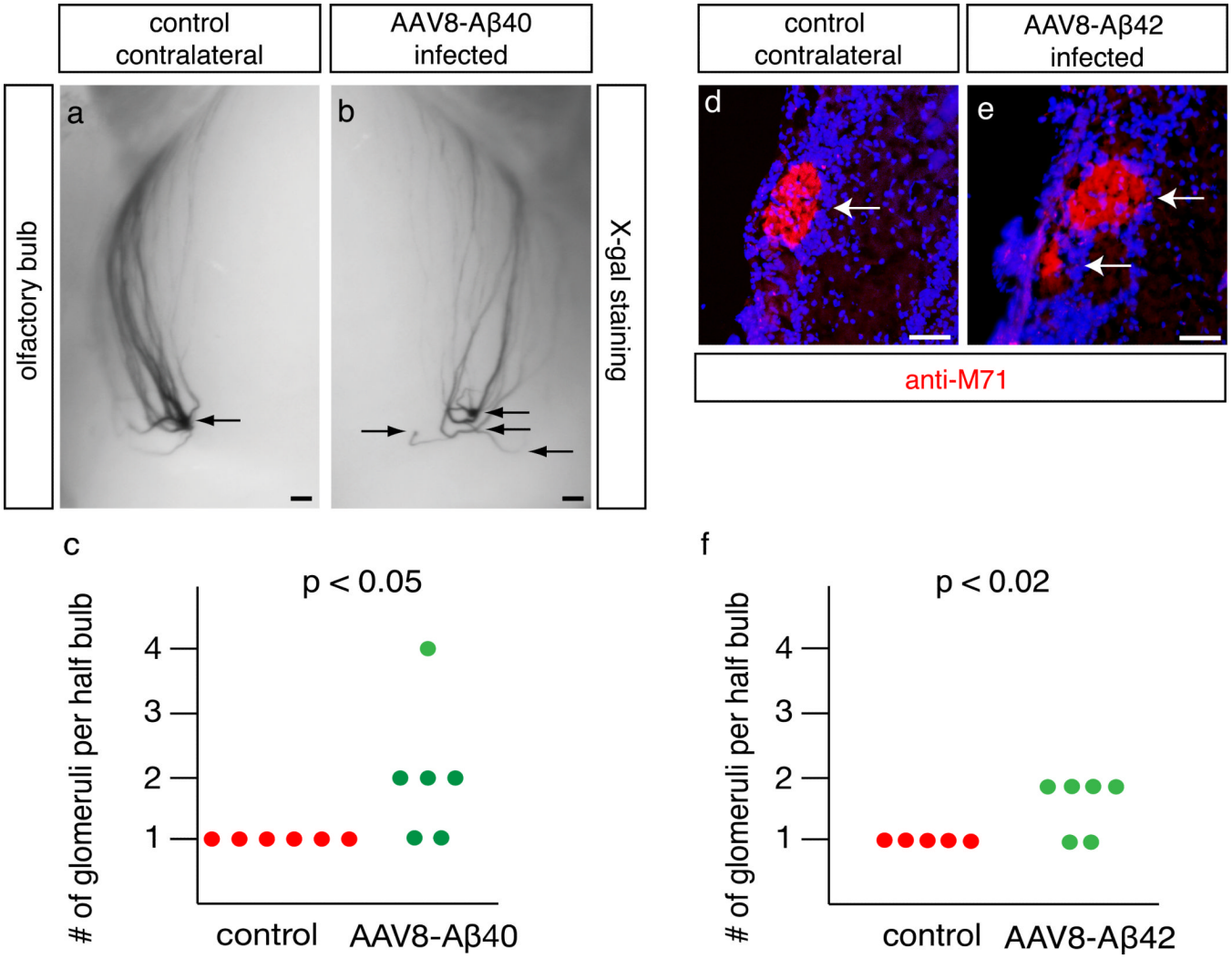

Figure 7. Aβ40 and Aβ42expression in the olfactory epithelium alters OSN axon targeting

(a–b) Representative images of the olfactory bulbs from an M71-ires-tauLacZ mouse infected with AAV8-BriAβ40 that were stained with X-gal (arrows indicate glomeruli receiving M71-expressing fibers). Scale bar = 200 μm. **(c)** Quantification of number of glomeruli receiving M71 expressing axons revealed a significant degree of mistargeting in the olfactory bulb ipsilateral to the AAV8-BriAβ40 infection ($p < 0.05$; two-tailed t test; n = 6 per genotype). **(d–e)** Representative images of the olfactory bulbs from a mouse infected with AAV8-BriAβ42 immunostained with antibody that recognizes M71 (arrows identify glomeruli revealing M71-expressing fibers). Scale bar = 100 μm. **(f)** Quantification of number of glomeruli receiving M71 expressing axons revealed a significant degree of mistargeting in the olfactory bulb ipsilateral to the AAV8-BriAβ42 infection ($p < 0.02$; two-tailed t test; n = 5 (controls); n = 6 (AAV8-BriAβ42).